

## Stellar prospects for FRB gravitational lensing

LIAM CONNOR<sup>1</sup> AND VIKRAM RAVI<sup>1</sup>

<sup>1</sup>*Cahill Center for Astronomy and Astrophysics, MC 249-17 California Institute of Technology, Pasadena, CA 91125, USA*

### ABSTRACT

Gravitational lensing of fast radio bursts (FRBs) offers an exciting avenue for several cosmological applications. However, it is not yet clear how many such events future surveys will detect nor how to optimally find them. We use the known properties of FRBs to forecast detection rates of gravitational lensing on delay timescales from microseconds to years, corresponding to lens masses spanning fifteen orders of magnitude. We highlight the role of the FRB redshift distribution on our ability to observe gravitational lensing. We consider cosmological lensing of FRBs by stars in foreground galaxies and show that strong stellar lensing will dominate on microsecond timescales. Upcoming surveys such as DSA-2000 and CHORD will constrain the fraction of dark matter in compact objects (e.g. primordial black holes) and may detect millilensing events from intermediate mass black holes (IMBHs) or small dark matter halos. Coherent all-sky monitors will be able to detect longer-duration lensing events from massive galaxies, in addition to short time-scale lensing. Finally, we propose a new application of FRB gravitational lensing that will measure directly the circumgalactic medium of intervening galaxies.

*Keywords:* fast radio bursts, cosmology, gravitational lensing

### 1. INTRODUCTION

Gravitational lensing is the deflection of light rays by intervening matter inhomogeneities between a source and an observer. If the deflection angle is sufficiently large, one can observe multiple images of the source. Each image will traverse a different path, leading to arrival time delays between the lensed copies. Therefore, variable sources and astrophysical transients allow one to detect gravitational lensing in the time domain. The differential arrival time of lensed images enable valuable cosmological applications, for example measuring the Hubble constant  $H_0$  with a technique known as time-delay cosmography (Refsdal 1964; Treu & Marshall 2016; Suyu et al. 2017).

Gravitational lensing in the time domain has primarily been observed in distant quasars (Vanderriest et al. 1989; Treu & Marshall 2016), the brightness of which fluctuates on human timescales due to their compact emitting regions. There are also several gravitationally lensed events or candidates from explosive transients (Oguri 2019) such as supernovae (Kelly et al. 2015; Rodney et al. 2021), gamma-ray bursts (GRBs) (Paynter et al. 2021), and gravitational waves events from coalescing binary black holes.

Fast radio bursts (FRBs) are bright, brief radio transients whose exact origins remain unknown (Petroff et al. 2019; Cordes & Chatterjee 2019). FRBs offer a uniquely precise probe of gravitational lensing in the time domain for two reasons: They are ubiquitous, with volumetric rates that may exceed those of core-collapse supernovae. And they are very short in duration, allowing for extraordinary measurements of the lensing time-delay. Typical bursts are  $\sim$ millisecond duration, but radio telescopes can preserve electric field information about the FRB on timescales of nanoseconds, well below the already-narrow pulse widths. This is in contrast to other time-delay lensing events, which are fundamentally limited in the delays—and therefore lens mass-scales—to which they are sensitive. In gravitational lensing, the image that arrives first will be brighter than subsequent copies. A schematic diagram of FRB lensing is shown in Figure 1.

In the past several years, a number of groups have explored the application of FRB gravitational lensing to cosmology and fundamental physics (Zheng et al. 2014; Li et al. 2018; Wucknitz et al. 2021; Chen et al. 2021b). Muñoz et al. (2016) outlined how searching for FRBs lensed on timescales of milliseconds would constrain the fraction of dark matter in massive compact halo objects (MACHOS), particularly in the mass range  $20\text{--}100 M_{\odot}$ . Relatedly, FRBs have been proposed as a probe of the mass distribution function of primordial black holes (PBHs) between  $10$  and  $10^3 M_{\odot}$  (Zhou et al. 2022). These methods are incoherent in that phase information about the electric field (i.e. the burst’s recorded complex voltage data) was not considered. Such methods have an identification problem because many FRBs repeat, so one must distinguish a genuine lensing event from a distinct burst from the same source. However, if voltage data—rather than just total intensity—of the burst are preserved, lensing delays can theoretically be detected down to the instrument’s inverse radio bandwidth ( $B \sim 1$  GHz or  $\Delta t \sim 10^{-9}$  s) (Eichler 2017; Pen 2018). Barring instrumental and propagation effects, lensed copies of the same burst ought to have identical waveforms. The same will not be true for intrinsically different bursts, whether from a repeating source or from a different FRB source along a similar sight line. The unprecedented access to time delays from nanoseconds to years means FRBs could probe lens mass scales from Jupiter-like objects up to massive galaxies, spanning many orders of magnitude in lens masses. Indeed, techniques for coherent time-delay gravitational lensing of compact sources such as pulsars and FRBs have been proposed for lensing by free-floating planets in the Milky Way (Jow et al. 2020). For longer time delays, propagation effects due to plasma, such as scattering, have deleterious effects on the coherent lensing signal. In those cases, being able to spatially resolve the multiple images using very-long baseline interferometry (VLBI) will enable new science for lenses that are galaxy-scale and above. The large range of time delays, image separations, and lens masses accessible to FRBs is shown in Figure 2.

Recently, these ideas have been developed more extensively and put into practice by the CHIME/FRB collaboration (Kader et al. 2022; Leung et al. 2022). The authors have built coherent methods for searching voltage data of CHIME/FRB sources for lensing events, which they refer to as “gravitational lens interferometry”. They are able to search for lensing delays between 2.5 ns and 100 ms, corresponding to  $10^{-4}\text{--}10^4 M_{\odot}$  lenses. They have applied these techniques to CHIME/FRB data to constrain the fraction of dark matter in PBHs using 172 bursts for which voltage data was preserved, accounting for decoherence from scattering (Leung et al. 2022). This amounted to 114 distinct sightlines, meaning a positive detection would have required a very high cosmic abundance of PBHs.

Despite the clear value of having a collection of gravitationally lensed FRBs from cosmological distances, it remains an open question how future surveys should optimally search for them or how many they will detect. The purpose of this work is to compare different telescope designs and to produce a realistic forecast for how many lensed FRBs future and current experiments might find. This allows us to discuss several science cases at a wide range of lensing timescales (and thus lens masses). We first offer a basic formalism for gravitational lensing in the time domain and calculate lensing optical depths at different mass scales. We then forecast total FRB detection rates on DSA-2000 (Hallinan et al. 2019), CHORD (Vanderlinde et al. 2019), and a coherent all-sky monitor (for example, BURSTT (Lin et al. 2022)<sup>1</sup>), finding they will detect tens of thousands of new FRBs. We combine these rates and their modelled redshift distributions with lensing optical depths to estimate the number of gravitationally lensed FRBs that will be detected on a range of timescales. We describe the science that can be done with lens masses of  $10^{-1}\text{--}10^{14} M_{\odot}$ . Finally we describe the application of FRB lensing to the circumgalactic medium (CGM), providing a clean measurement of halo gas properties along different lines of sight.

<sup>1</sup> <https://www.asiaa.sinica.edu.tw/project/burstt.php>

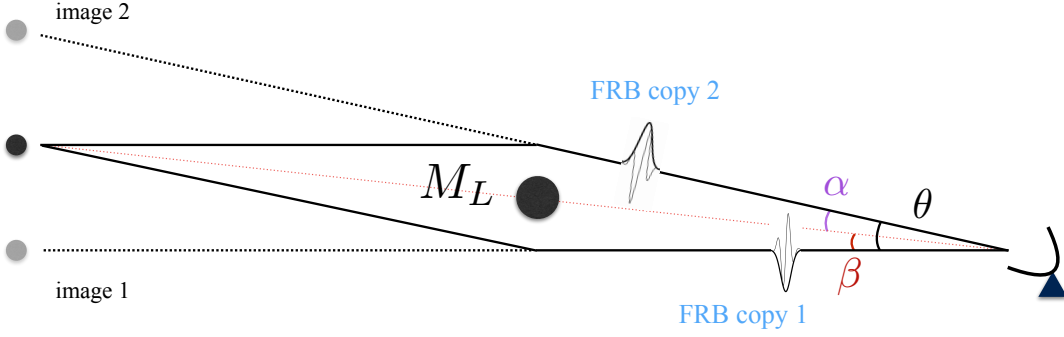


**Figure 1.** Diagram of fast radio burst gravitational lensing.

## 2. GRAVITATIONAL LENSING BACKGROUND

If a source is at a true sky position,  $\beta$ , its image will appear at  $\theta$ , deflected by the angle  $\alpha$  in the presence of a gravitational lens. The mapping between the true and apparent source position is given by the lens equation,

$$\beta = \theta - \alpha(\theta). \quad (1)$$

The deflection angle,  $\alpha$ , is given by an integral of the projected surface mass density,  $\Sigma(\theta)$  over angular position,

$$\alpha(\theta) = \frac{1}{\pi} \int d\theta' \frac{|\theta - \theta'|}{|\theta - \theta'|^2} \frac{\Sigma(\theta')}{\Sigma_{cr}}. \quad (2)$$

Here  $\Sigma_{cr}$  is the critical surface density and is given by the geometry of the lensing system,

$$\Sigma_{cr} = \frac{c^2}{4\pi G} \frac{D_s}{D_l D_{ls}}, \quad (3)$$

where  $D_s$ ,  $D_l$ , and  $D_{ls}$  are the distances to the source, the lens, and the distance between the lens and the source, respectively.  $\Sigma_{cr}$ , and therefore the solution to the lens equation, also depend on the constituents of the Universe because  $D_s$ ,  $D_l$ , and  $D_{ls}$  are all angular diameter distances.

The Lens Equation is non-linear in  $\theta$ , so there can be more than one  $\theta$  that satisfies Eq 1. Hence, gravitational lenses produce multiple images or multiple lensed copies in time. A special case is when the source is directly behind the lens where  $\beta = 0$ . In that scenario, the deflection angle is equal to the image position. That angle is known as the Einstein radius,  $\theta_E = \alpha$ .

The next useful quantity for our purposes is the lensing optical depth, which is the probability that a source at redshift  $z_s$  is lensed. It will be an integral of the cross sections ( $\sigma \approx \pi \theta_E^2$ ) of all lenses between the observer and the source.

$$\tau(z_s) = \int_0^{z_s} dz_l \int n(\sigma, z_l) \sigma \frac{d^2V}{d\Omega dz_l} \quad (4)$$

Here,  $n(\sigma, z_l)$  is the number density of sources at redshift with cross-sectional area  $\sigma$  and  $\frac{d^2V}{d\Omega dz_l}$  is the comoving volume element per redshift per steradian.

We are concerned with the rate of FRB lensing events, for which we must incorporate the source redshift distribution. Assuming an FRB detection rate per redshift (in the absence of lensing) of  $\mathcal{R}_{det}(z_s)$ , the rate of observed lensing events,  $\mathcal{R}_L$ , will be the following:

$$\mathcal{R}_L = \int_0^\infty dz_s \mathcal{R}_{det}(z_s) \int_0^{z_s} dz_l \int B(\gamma) n(\sigma, z_l) \sigma \frac{d^2V}{d\Omega dz_l}. \quad (5)$$

The parameter  $B$  accounts for a phenomenon known as magnification bias (Turner 1980). Since gravitational lensing can magnify the intensity of lensed copies, faint sources that are otherwise below a survey's detection threshold can

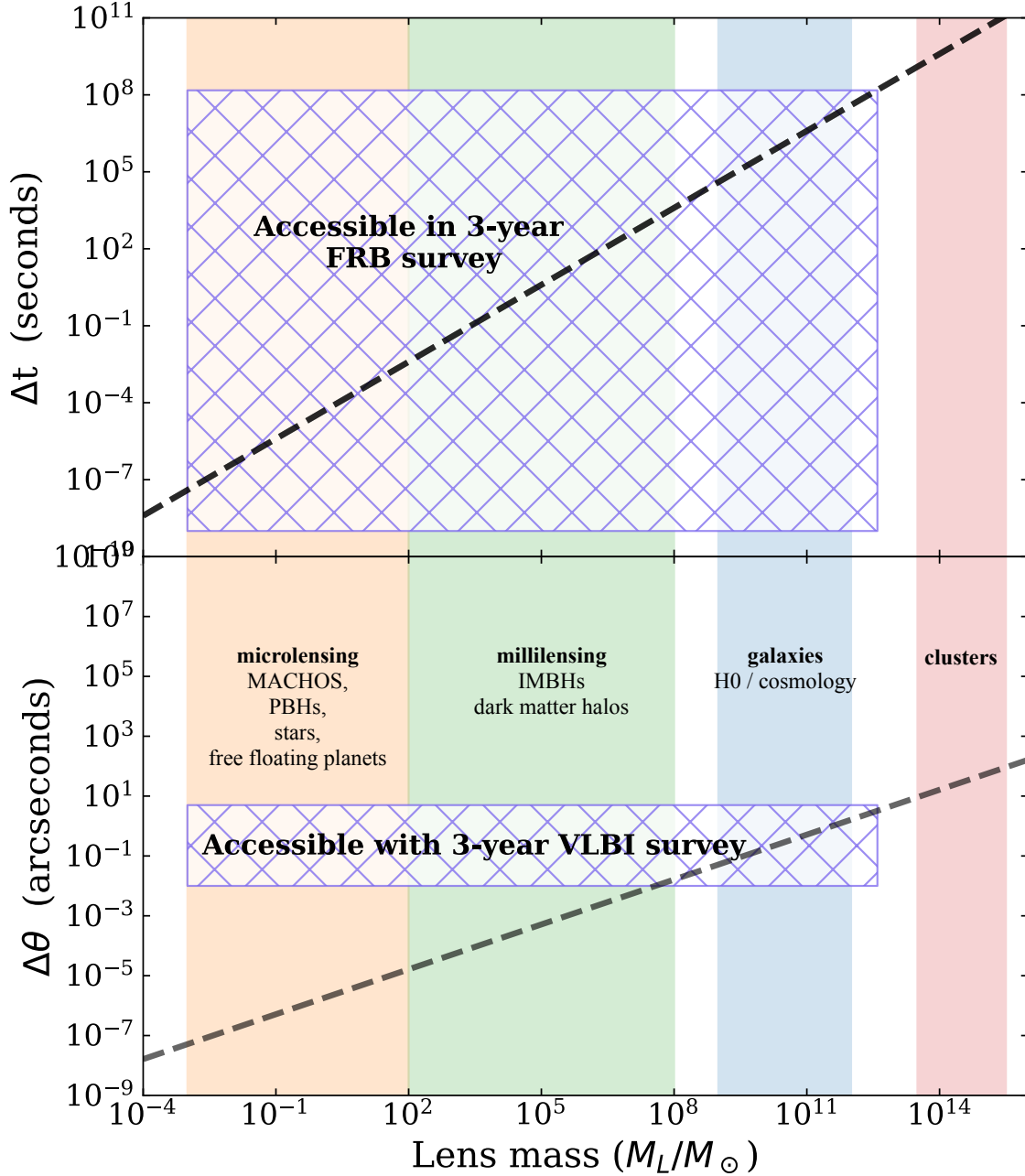


**Figure 2.** The phase space of FRB gravitational lensing for a source at  $z = 1$  and lens at  $z = 0.5$ . The dashed black curves in the top and bottom panels show the fiducial time delay and image separation, respectively, as a function of lens mass. The solid shaded regions give examples of the types of lenses at each mass scale.

be made observable. This increases the number of lensed objects and must be accounted for when computing optical depth. Assuming a power-law luminosity function,  $N(L) \propto L^{-\gamma}$ , and a singular isothermal sphere (SIS) lens,

$$B(\gamma) = \frac{2^\gamma}{3 - \gamma}. \quad (6)$$

The equation shows magnification bias is stronger for steeper luminosity functions, i.e. large  $\gamma$ . This is because steep power-laws indicate an abundance of low-luminosity sources that can only be observed in the presence of lensing magnification for a flux-limited survey.

Evidently, the main ingredients that impact the detection of FRB lensing will be the abundance of lenses, the mass distribution of those lenses, and the redshift distribution of FRBs that a given survey observes. Another important factor for transient lensing will be sky coverage and observing strategy, which is captured by the “time-delay selection function”.

### 2.0.1. Time-delay selection function

In the image-domain, only one image is needed to search for evidence of gravitational lensing. But for time-domain events such as FRBs, GRBs, SNe, or time-variable AGN, one must be pointing at the same patch of sky when the lensed signal arrives. This poses a challenge for transient gravitational lensing. We call the probability that the lensed copy will be in the telescope’s field-of-view (FoV)  $P_{\text{FoV}}(\Delta t)$ . This determines the likelihood that a lensed image will be recorded by a time-domain survey. When calculating the true detection rate of lensed FRBs with Eq 5, we must multiply the integrand by  $P_{\text{FoV}}(\Delta t)$ .

For a transit instrument with east west beamwidth,  $\theta_{\text{EW}}$ , lensed copies will be recorded if the delay is less than a beam crossing time,  $t_{\text{trans}}$ . If the delay is greater than a transit time but less than one day, it cannot be detected. For delays longer than one day, the probability of detecting the lensed copy is the fractional sky coverage, or  $\frac{\theta_{\text{EW}}}{2\pi}$ . Examples of such FRB surveys are CHIME/FRB (CHIME/FRB Collaboration et al. 2018), DSA-110<sup>2</sup>, and CHORD (Vanderlinde et al. 2019). The probability that the lensed copy will be in the beam is therefore,

$$P_{\text{FoV}}(\Delta t) = \begin{cases} 1 & \Delta t \leq t_{\text{trans}} \\ 0 & t_{\text{trans}} < \Delta t < 1 \text{ day} \\ \frac{\theta_{\text{EW}}}{2\pi} & \Delta t \geq 1 \text{ day} \end{cases} \quad (7)$$

For CHORD,  $P_{\text{FoV}}(\Delta t \geq 10^5 \text{ s}) \approx 9 \times 10^{-3}$  at the center of the band, assuming the instrument is parked at the same declination. For a steerable all-sky survey such as DSA-2000,  $P_{\text{FoV}}(\Delta t) = 1$  for  $\Delta t$  less than a pointing time. For longer time-delays,  $P_{\text{FoV}}(\Delta t)$  will be roughly the fraction of time spent on each patch of sky, or the primary beam size divided by  $3\pi$  ( $P_{\text{FoV}}(\Delta t \geq 10^3 \text{ s}) \approx 3 \times 10^{-4}$  on DSA-2000). In practice, CHIME/FRB, CHORD, DSA-110, and DSA-2000 will have a difficult time detecting gravitational lensing events caused by massive galaxies unless special survey strategy is undertaken. Instead, they will be able to search for lensing by compact objects and halos with  $M_L \lesssim 10^8 M_\odot$ .

An ultra-widfield FRB survey, which observes a similar region of sky at all times, will be able to search for lensing delays up to the survey duration. We refer to such surveys as coherent all-sky monitors, or CASMs, of which the proposed experiment BURSTT is an example (Lin et al. 2022). However, such a design will inevitably be less sensitive than DSA-2000 or CHORD and will therefore probe a more nearby population of FRBs. In Section 4 we compare this trade-off. Another way to access longer lensing time-delays is to point one’s telescope at the north or south celestial pole such that the same field is observed at all times or observe a circumpolar region with a tracking telescope.

### 2.1. Lensing by a point mass

We start with the simplest possible mass distribution, that of a point mass. We calculate both the Einstein radius and typical time-delay for a cosmological source. This will be relevant for stellar lenses, primordial black holes / MACHOS, and intermediate-mass black holes. For a point mass, the Einstein radius scales as the square root of mass as,

$$\theta_E = \sqrt{\frac{4GM}{c^2} \frac{D_{ls}}{D_l D_s}} \quad (8)$$

$$\approx 1.6'' \times 10^{-6} \left(\frac{M}{M_\odot}\right)^{1/2} \left(\frac{D_l D_s / D_{ls}}{3 \text{ Gpc}}\right)^{-1/2} \quad (9)$$

To compute a time-delay between images, we follow Oguri (2019) by defining a fiducial time-delay,  $\Delta t_{\text{fid}}$ , which is the difference in arrival time between the unlensed line-of-sight and an image deflected by  $\theta_E$ . In practice, the true

<sup>2</sup> <https://www.deepsynoptic.org/team-110>

observable between images  $i$  and  $j$  is the difference between their time-delays, i.e. we measure  $\Delta t_{ij} = \Delta t_i - \Delta t_j$ . It is still useful to consider the typical lensing delay timescale. This is given by,

$$\Delta t_{fid} \approx 20 \mu\text{s} \times (1 + z_l) \left( \frac{M}{M_\odot} \right). \quad (10)$$

The point lens will produce images separated by the following,

$$\theta_\pm = \frac{1}{2} \left( \beta \pm \sqrt{\beta^2 + 4\theta_E^2} \right), \quad (11)$$

where  $\beta$  is angular impact parameter. The time delay will be,

$$\Delta t = \frac{4GM_l}{c^3} (1 + z_l) \left( \frac{y}{2} \sqrt{y^2 + 4} + \log \left( \frac{\sqrt{y^2 + 4} + y}{\sqrt{y^2 + 4} - y} \right) \right), \quad (12)$$

where  $y \equiv \beta/\theta_E$  (Muñoz et al. 2016).

In order to calculate the lensing optical depth, one must usually account for the fact that the area is an annulus between  $y_{min}$  and  $y_{max}$  rather than simply a cross section of  $\pi\theta_E^2$ . The areal scale of the lens is then,

$$\sigma(z_l, M_l) = \frac{4\pi G M_l}{c^2} \frac{D_l D_{ls}}{D_s} (y_{max}^2 - y_{min}^2). \quad (13)$$

Here,  $y_{max}$  is set by the largest acceptable image pair flux ratio. The minimum value,  $y_{min}$ , is set by the minimum detectable time delay between the two images. Unlike with GRBs (Paynter et al. 2021, e.g.) or previous incoherent treatments of FRB lensing (Muñoz et al. 2016; Zhou et al. 2022), we assume a coherent lensed search that can find delays below the pulse width scale,  $\Delta t \ll t_{FRB}$  (Eichler 2017; Wucknitz et al. 2021). This renders  $y_{min}$  negligible so we set it to zero going forward. The source number density is,

$$n(z_l, M_l) = \frac{\rho_c f_l \Omega_c}{M_l} (1 + z)^3, \quad (14)$$

where  $\rho_c$  is the critical density of the Universe,  $\Omega_c$  is the cosmological density parameter of cold dark matter at  $z = 0$ , and  $f_l$  is the fraction of dark matter in compact lenses (e.g. in primordial black holes or IMBHs). Combining these terms, we find that the lensing optical depth is independent of the mass of compact halos. It is given by,

$$\tau(z_s) = \frac{3}{2} f_l \Omega_c H_0^2 \int_0^{z_s} dz_l B \frac{(1 + z_l)^2}{c H(z_l)} \frac{D_l D_{ls}}{D_s} y_{max}^2. \quad (15)$$

As a useful guide, the classic Press-Gunn approximation relates the cosmic abundance of lenses to their mean optical depth as  $\tau \approx \Omega_l$  for high redshift sources, where  $\Omega_l$  is the cosmological parameter for that type of point-mass lens (Press & Gunn 1973). For lower redshifts, the scaling is closer to  $\tau \approx \Omega_l \left(\frac{z}{2}\right)^2$  (Narayan & Bartelmann 1996). Notably, the relation is independent of lens mass.

In Figure 3 we plot lensing probability curves for two point mass scenarios as a function of redshift. The dotted curve assumes 0.1% of dark matter is made from compact halos and the dot-dashed curve assumes this number is  $10^{-4}$ , both of which are currently permitted in the relevant lens mass range. Each uses a magnification bias of 2.

## 2.2. Strong lensing by massive galaxies

The lensing optical depth for distant objects is dominated by the dark matter halos of massive foreground galaxies. Lensing halos are typically taken to be singular isothermal spheres (SIS) or ellipsoids (SIE). These objects are parameterized by their Einstein radius given by,

$$\theta_E = 4\pi \frac{\sigma_v^2}{c^2} \frac{D_{ls}}{D_s}, \quad (16)$$

where  $\sigma_v$  is the halos' velocity dispersion. For reference, with  $\sigma_v = 200 \text{ km s}^{-1}$  and  $D_{ls}/D_s = 0.426$ , the Einstein radius is roughly  $0.5''$ , or a typical image separation of one arcsecond. The optical depth is then,

$$\tau(z_s) = \int_0^{z_s} dz_l \int d\sigma_v B(\gamma) \phi(\sigma_v, z_l) \frac{d^2 V}{d\Omega dz_l} \pi \theta_E^2(\sigma, z_l, z_s) D_l^2, \quad (17)$$

where  $\frac{d^2V}{d\Omega dz_l}$  is the differential comoving volume at  $z_l$  and  $\phi(\sigma, z_l)$  is the number density of galaxies with velocity dispersion  $\sigma$ , also known as velocity dispersion function (VDF).

To model the lensing optical depth from massive galaxies we use a model based on a recent empirical galaxy VDF (Yue et al. 2022). Another quick approximation for lensing probability is given by (Oguri 2019),

$$\tau(z_s) = \frac{5 \times 10^{-4} z_s^3}{(1 + 0.041 z_s^{1.1})^{2.7}} \quad (18)$$

Clearly, the probability that a given FRB is lensed by an intervening galaxy is strongly dependent on redshift, rising as  $z^3$  for  $z \lesssim 1.5$ . This is apparent in the solid black curve of Figure 3. Therefore, any FRB survey that hopes to detect gravitational lensing would benefit from detecting distant bursts.

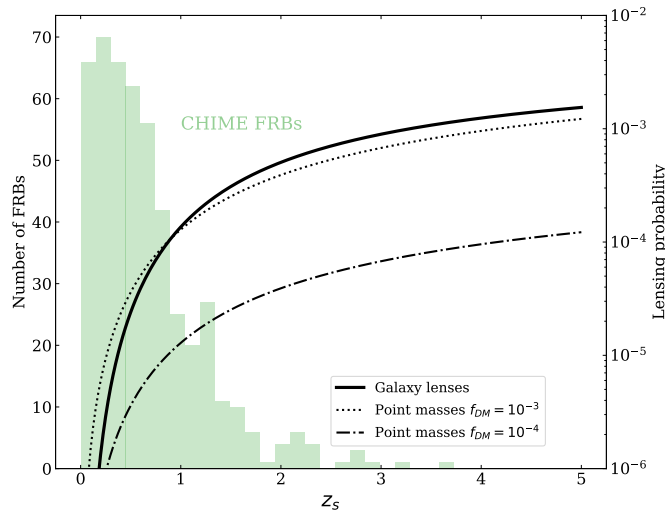


**Figure 3.** The modeled CHIME/FRB redshift distribution (green histogram, left vertical axis) and the probability that a source at redshift  $z_s$  is lensed (right vertical axis). The lensing optical depth,  $\tau(z_s)$  increases quickly with redshift such that most CHIME/FRBs have a very low chance of strong lensing. We have assumed a magnification bias  $B = 2$ .

### 2.3. Coherent gravitational lensing

Radio telescopes measure directly the electric field of incoming electromagnetic waves, sampling voltages roughly one billion times per second for  $\sim$ decimeter wavelengths. FRB search pipelines “detect” this data by effectively squaring the voltages. They then downsample in time and frequency to a manageable data rate, and search the lower-resolution intensity data for dispersed pulses. Many surveys now preserve the raw voltage data with a buffer that can be triggered and saved to disk, allowing astronomers to analyze the radio pulse’s waveform. This is true for current surveys such as CHIME/FRB (Michilli et al. 2021), ASKAP (Bannister et al. 2019), DSA-110, and will be true for nearly all upcoming surveys.

Having access to the waveform itself is a major advantage for gravitational lensing (Eichler 2017). If two pulses arrive from a similar sky position but at different times, their voltage timestream can be cross-correlated to test whether they are the same pulse (i.e. lensed copies of one another) and not just repeat bursts from the same source. Crucially, this can be done on timescales shorter than the burst width using an autocorrelation. A “single” FRB can be correlated with itself, and one can search for power at non-zero time-lags, down to delays of the reciprocal bandwidth (nanoseconds). Similar techniques have been successfully applied to the voltage timestreams of giant pulses, effectively descattering Galactic pulsars (Main et al. 2017). Despite the theoretical limit of  $1/\Delta B$ , for this paper we follow Wucknitz et al. (2021) and assume a practical time-lag (lensing delay) lower limit of 1 microsecond.

There are a number of practical issues related to coherent gravitational lensing searches. These include inverting the instrument’s polyphase filterbank, removing dispersion measure (DM) with high precision, radio frequency interference (RFI), and the deleterious effects of interstellar scattering. However, these are beyond the scope of our work and we point the reader to a detailed description and application of coherent lensing searches, or FRB gravitational lens

interferometry, by the CHIME/FRB collaboration (Kader et al. 2022; Leung et al. 2022). We are here focused on detection rates and applications to cosmology and fundamental physics for upcoming surveys.

### 3. FRB SURVEYS

#### 3.1. Detection rates

Despite considerable advances in constraining the source counts and all-sky rate of FRBs, forecasting detection rates on new surveys remains challenging (Connor 2019). This is due to disparate RFI environments and detection pipelines between telescopes as well as the unknown frequency dependence of the FRB rate. However, thanks to a large collection of FRBs from CHIME at 400–800 MHz and  $\mathcal{O}(100)$  events from surveys near 1.4 GHz, we are no longer limited by small number statistics. These surveys have also implemented careful injection tests to measure pipeline completeness, thus we are in a far better position to estimate future survey detection rates than we have ever been in before. We also now have cumulative rate measurements spanning more than three orders of magnitude in flux density threshold, giving us a handle on the abundance of FRBs at 10 mJy up to 100 Jy (Niu et al. 2021; Shannon et al. 2018; James et al. 2019). Figure 4 shows current FRB source counts and effective detection rates for several surveys. FAST has shown that the milliJansky radio sky is full of FRBs (Niu et al. 2021), which is promising for sensitive future surveys such as DSA-2000 and CHORD.

Here we extrapolate from known surveys to estimate the detection rates at DSA-2000, CHORD, and the Omniscope. This will allow us to forecast gravitational lensing science that they can do. We start with the standard simplified rate equation for a transient survey, which is the product of the survey’s FoV,  $\Omega$  and areal source density above some minimum flux density,  $n(> S_{min})$ ,

$$\mathcal{R} = \Omega n(> S_{min}). \quad (19)$$

Assume a survey  $k$  has a system-equivalent flux density,  $SEFD_k$ ,  $n_{p,k}$  polarizations, and radio bandwidth,  $B_k$ . We can now extrapolate from a survey  $l$  with a known detection rate of survey  $\mathcal{R}_l$ , giving,

$$\mathcal{R}_k = \mathcal{R}_l \frac{\Omega_k}{\Omega_l} \left( \frac{SEFD_l}{SEFD_k} \sqrt{\frac{B_k n_{p,k}}{B_l n_{p,l}}} \right)^\alpha. \quad (20)$$

In Table 1 we list the parameters for current and upcoming telescopes; for existing surveys we have estimated the FRB detection rates. For parabolic reflectors, we assume  $\Omega \approx 1.13 \left(\frac{\lambda}{D}\right)^2$ . Both DSA-2000 and CHORD utilize ultrawideband receivers, forcing us to make a choice about our treatment of the frequency dependence of FRB rates. Rather than modelling an FRB spectral index, we can break the surveys up into two sub-bands that are assumed to find different FRBs. This is partly because FRBs are often band-limited and because the FoV mismatch across an ultrawideband survey: For CHORD, the primary beam at the lowest frequencies is 25 times larger than at the top, so most FRBs arriving in the beam at the bottom of the band will not be detected at the top of the band, even if the pulses spanned  $\sim 1.2$  GHz. We combine empirical rates at 1.4 GHz from FAST (Niu et al. 2021) and Apertif (van Leeuwen et al. 2022) with the CHIME/FRB detection rates at 600 MHz. We extrapolate directly from the CHIME rate (below 1 GHz) and from the FAST/Apertif rate (above 1 GHz, denoted by subscript “L”). Breaking an ultra-wideband into two sub-bands, the rate equation becomes,

$$\mathcal{R}_k = \mathcal{R}_{CH} \frac{\Omega_k}{\Omega_{CH}} \left( \frac{SEFD_{CH}}{SEFD_k} \sqrt{\frac{B_k}{B_{CH}}} \right)^\alpha + \mathcal{R}_L \frac{\Omega_k}{\Omega_L} \left( \frac{SEFD_L}{SEFD_k} \sqrt{\frac{B_k}{B_L}} \right)^\alpha \quad (21)$$

#### 3.1.1. DSA-2000

The DSA-2000 is a proposed wide-field radio camera that will have 2000×5 m steerable antennas and will observe between 700–2000 MHz (Hallinan et al. 2019). It will have a system-equivalent flux density (SEFD) of 2.5 Jy and a field-of-view (FoV) given by,

$$\Omega = 10.8 \left( \frac{\nu}{1100 \text{ MHz}} \right)^{-2} \text{ deg}^2. \quad (22)$$

Utilizing the full FoV for pulsar and FRB search requires forming and searching a large number of beams, which is computationally challenging. This number is given by  $N_{beam} = (d_{max}/D)^2$ , where  $d_{max} \approx 15.3$  km is the longest

Survey	FoV (deg <sup>2</sup> )	SEFD (Jy)	Frequency (MHz)	$N_{ant}$	Diameter (m)	Rate (year <sup>-1</sup> )	$\langle z_s \rangle$
CHIME	200	50	400–800	1024	N/A	500–1000	0.5
Apertif	9	75	1220–1520	10	25	30–90	0.5
FAST	0.019	1.33	1000–1500	1	500/300 <sup>†</sup>	4–40	1.35
<i>DSA-2000</i>	18–3	2.5 / 6 <sup>†</sup>	700–2000	2000	5	1000–4000	1.2
<i>CHORD</i>	72–2.9	9	300–1500	512	6	1100–6000	1.0
<i>CASM</i>	5000	50	400–800	5000	N/A	12500–25000	0.5

**Table 1.** The parameters for current and upcoming (italicized) FRB surveys. The rate column gives the FRB detections per one year on sky, and not the effective detection rate which requires multiplying by observing duty-cycle. The final column,  $\langle z_s \rangle$ , is the mean redshift. This is estimated from the DMs of current surveys and from modelling for the three upcoming surveys (see Section 3.2).

<sup>†</sup> corresponds to an effective value for the FRB search.

baseline and  $D = 5$  m is dish diameter, giving  $N_{beam} \approx 10^7$ . For a reduced number of beams there is a trade-off between the effective FoV that can be searched,  $\Omega_{eff}$ , and effective sensitivity. If baselines longer than  $d_{cut}$  are discarded, the effective SEFD will be  $2.5 \text{ Jy} \sqrt{f(d < d_{cut})}^{-1}$ , where  $f(d < d_{cut})$  is the fraction of baselines shorter than  $d_{cut}$ . The effective FoV at 1100 MHz will then be,

$$\Omega_{eff} = \min \left\{ 10.6 \text{ deg}^2, N_{beam} \times 1.13 \left( \frac{c/1100 \text{ MHz}}{d_{cut}} 180/\pi \right)^2 \right\}, \quad (23)$$

where  $N_{beam}$  is the total number of beams that can be searched. We use a *min* operator because we cannot usefully search beyond the instrument’s primary beam. Assuming Euclidean source counts, detection rate is maximized when  $d_{cut}$  is such that the full primary beam is tiled by  $N_{beam}$ . We find that if DSA-2000 can afford to search  $10^6$  beams,  $d_{cut}$  should be chosen such that the synthesized beamwidth is 11” and the effective SEFD is 5 Jy. For the current antenna configuration, this corresponds to  $d_{cut} \approx 4.1$  km. For the remaining forecasts, we assume that DSA-2000 will have SEFD=6 Jy and  $\Omega_{eff} = 10.6 \text{ deg}^2$  at 1100 MHz. We further assume that DSA-2000 will only search for FRBs between 700 MHz and 1600 MHz.

Following Equation 21, we find that DSA-2000 will detect 830–4600 FRBs per year. Over the course of its nominal five year survey (and an estimated four years on sky), this would result in  $\mathcal{O}(10^4)$  localized FRBs in which to search for gravitational lensing.

### 3.1.2. CHORD

CHORD is funded transit radio telescope that is preparing for construction (Vanderlinde et al. 2019). The FRB search on CHORD will use  $512 \times 6$  m antennas organized in a compact grid, comprising the array’s core. CHORD employs ultra-wideband antennas covering 300–1500 MHz and has an expected SEFD of 9 Jy. Its FoV is given by,

$$\Omega = 7.7 \left( \frac{\nu}{1100 \text{ MHz}} \right)^{-2} \text{ deg}^2. \quad (24)$$

Though it has less collecting area and sensitivity than DSA-2000, the dense antenna configuration of its core is optimal for searching the full FoV at nominal sensitivity. It will only need to form and search 512 beams. Two outrigger stations separated from the core by more than  $10^3$  km allow for VLBI localization of FRBs at milli-arcsecond-level precision. CHORD has an unprecedented 5:1 radio bandwidth that will require sub-band searching, due to the FoV mismatch as a function of frequency (Vanderlinde et al. 2019). Rather than break the full band into just two sub-bands as we have done with DSA-2000, we choose to sum FRB detections in three geometric sub-bands: 300–515 MHz, 515–880 MHz, and 880–1500 MHz. In the top sub-band, between 880–1500 MHz, we extrapolate from the FAST detection rate because of the match between sensitivity and frequency between the two telescopes. In the bottom two sub-bands, we extrapolate from CHIME/FRB and use  $\alpha = 1.5$ . We find that CHORD will discover 1000–6000 FRBs per year, all with voltage dumps and precise localizations.

### 3.1.3. A coherent all-sky monitor (CASM)

The logical endpoint of the large- $N$  small- $D$  paradigm for radio interferometers is an aperture array, in which radio receivers are pointed directly at the sky without a light-focusing dish. A dense aperture array with a large number of

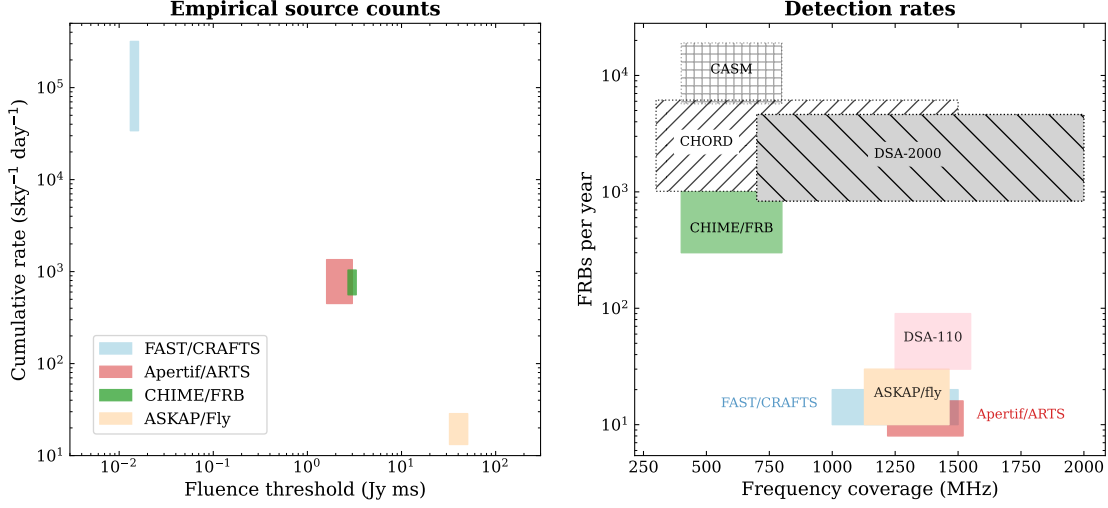


**Figure 4.** All sky FRB rates and survey detection rates. The left panel shows the cumulative all-sky event rate of FRBs as a function of fluence threshold. The long baseline in fluence provided by FAST and ASKAP in Fly’s Eye mode allow for source counts constraints over nearly four orders of magnitude. The right panel shows *effective* detection rates and frequency coverage for four surveys currently on sky (solid boxes), as well as three upcoming surveys for which we have run forecasts. The FRB detection rate here includes observing duty-cycle. For example Apertif only observed  $\sim 25\%$  of the time so its effective detection rate was one quarter of its rate per time on sky.

feeds could survey thousands of square degrees simultaneously at high sensitivity, detecting an enormous number of FRBs. Such an instrument would be a coherent all-sky monitor, so we refer to this hypothetical survey throughout the remainder of the paper with the acronym “CASM”.

Front-end electronics and digitization would be challenging for such a large number of antennas, but beamforming would be made feasible by FFT beamforming (Peterson et al. 2006; Tegmark & Zaldarriaga 2009). For example, a feed with a  $\sim 70$  deg opening angle would have a FoV that is  $\sim 10^4$  times larger than that of Parkes and 25 times greater than CHIME. Each feed would have an effective collecting area of  $\lambda^2$ . To build up the same collecting area as CHIME at 600 MHz, roughly 25,000 feeds would be required.

Dense aperture arrays already exist, but not with the ability to use the full FoV coherently. For example, the Electronic Multi Beam Radio Astronomy ConcEpt (EMBRACE) was designed and constructed in the Netherlands in order to demonstrate phased array technology for the Square Kilometer Array (SKA) (Kant et al. 2009). EMBRACE has over 20,000 elements and roughly 160 m<sup>2</sup> of collecting area. It uses hierarchical analog beamforming. The dense aperture array design once proposed for the SKA, and for which EMBRACE was a pathfinder, will not be built. This has led some work to mistakenly infer that SKA-Mid will detect as many as  $10^7$  FRBs per year (Hashimoto et al. 2020; Chen et al. 2021a), based on the dense aperture array proposal.

There is at least one proposed FRB survey that falls within the dense aperture array design. The Bustling Universe Radio Survey Telescope in Taiwan (BURSTT) is an example of a coherent all-sky monitor that would have a high FRB detection rate and outriggers for localization (Lin et al. 2022). It has been considered explicitly in the context of coherent gravitational lensing. Beyond the high FRB detection rate afforded by an ultra-widefield telescope, CASM experiments can go after longer time-delays from lensing because a large patch of sky can be observed continuously. Outrigger stations will provide VLBI localizations that will enable new applications of FRB gravitational lensing by massive galaxies. BURSTT-2048 is expected to have an SEFD of 600 Jy and will spend a significant portion of its time near the north celestial pole (Lin et al. 2022).

For the purposes of this paper, we will assume a future CASM survey that has the sensitivity of CHIME/FRB. The SEFD is taken to be 50 Jy, observing in the band 400–800 MHz, with a FoV of 5,000 deg<sup>2</sup>. In other words, a CHIME/FRB-like survey but with  $25 \times$  the sky coverage. These survey parameters make forecasting FRB detection rates very simple, because it will be roughly 25 times the CHIME/FRB detection rate; one does not have to assume anything about spectral index nor source counts. The major uncertainty, instead, is whether such an interferometer

can be built to spec. We do not attempt to model system performance uncertainty, and instead use CASM as a placeholder for an all-sky survey with CHIME/FRB sensitivity observing at 400–800 MHz. The inferred detection rate of CASM would be 7,500–25,000 FRBs per year, reaching  $\mathcal{O}(10^5)$  FRBs after 5–10 years on sky.

### 3.2. Redshift distribution

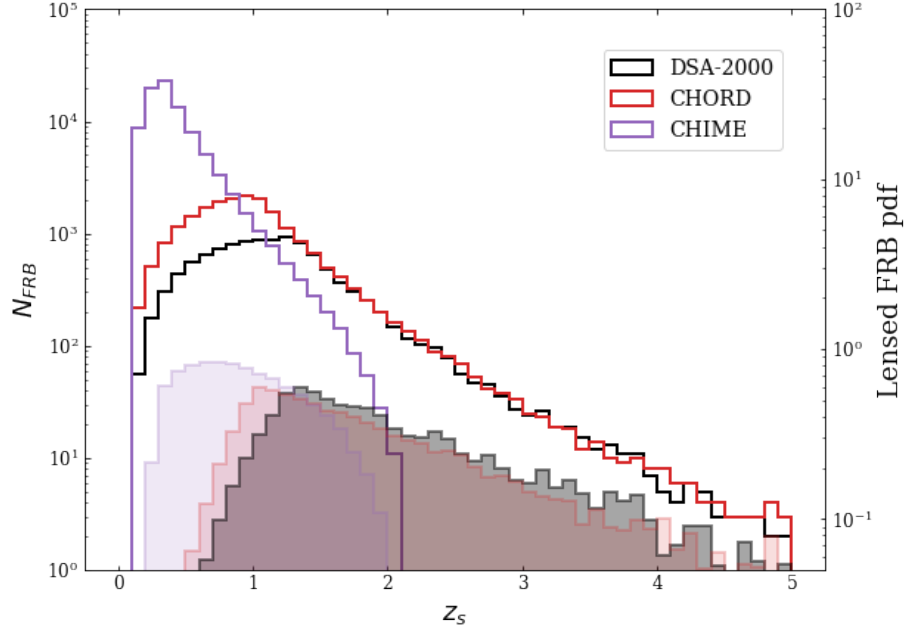


**Figure 5.** The modeled redshift distributions of DSA-2000, CHORD, and CASM. The latter has the highest total detection rate, but DSA-2000 and CHORD will probe higher redshifts thanks to their high sensitivity. The shaded histograms represent each survey’s lensing probability density function.

The number of lensed FRBs in upcoming surveys will be a strong function of the source redshift distribution: lensing optical depth increases as the cube of redshift for  $z_s \lesssim 1.5$  for strong galaxy lensing. It is imperative that a forecast for the lensing detection rate includes a realistic model for the FRB redshift distribution. To address this, we make use of two important relationships. One is the dependence of observed extragalactic dispersion measure ( $DM_{ex}$ ) on redshift, and the other is the relationship between distance and burst brightness.

Macquart et al. (2020) established that FRBs with higher  $DM_{ex}$  are typically farther away, as expected if the IGM dominates dispersion. The so-called “Macquart relation” is given by the following,

$$\langle DM_{IGM}(z) \rangle \approx 865 z \text{ pc cm}^{-3}. \quad (25)$$

While this approximate linear relationship holds, we caution that the  $DM_{ex}$  dependence on  $z$  is impacted by the host galaxy DM distribution (James et al. 2022). We solve for  $z$  with,

$$DM_{ex} = 865 z + \frac{100}{1+z} \text{ pc cm}^{-3}, \quad (26)$$

which can be rearranged into a quadratic equation,

$$865 z^2 + (DM_{ex} - 865)z + DM_{ex} - 100 = 0. \quad (27)$$

The CHIME/FRB Catalog 1 (CHIME/FRB Collaboration et al. 2021) estimates extragalactic DM by subtracting the expected contribution of the Milky Way along that line of sight from the observed DM. We use these to solve for  $z$  in Equation 27. The resulting redshift distribution for the first CHIME/FRB release is shown in Figure 3

	DSA-2000	CHORD	CASM	CHIME/FRB
$N_{FRB}$ (5 years)	4,000–16,000	4,400–24,000	50,000–100,000	2,500–5,000
$N_{lens,*}$	6–32	8–48	50–100	0.5–5
$f_{PBH}$ ( $0.1\text{--}100 M_{\odot}$ ) <sup>†</sup>	$\leq 1.2 \times 10^{-3}$	$\leq 1.1 \times 10^{-3}$	$\leq 1.0 \times 10^{-3}$	$\leq 0.06$
$\Omega_{IMBH}$ ( $10^3\text{--}10^5 M_{\odot}$ ) <sup>*</sup>	$\leq 10^{-2}$	$\leq 10^{-2}$	$\leq 10^{-3}$	$\leq 10^{-1}$
$N_{lens,IMBH}$ ( $10^3\text{--}10^5 M_{\odot}$ ) <sup>*</sup>	0.1–7.3	0.1–7.0	0.3–7.2	0.01–0.29
$N_{lens,gal}$ ( $10^{10}\text{--}10^{12} M_{\odot}$ ) <sup>**</sup>	-	-	5–40	-

**Table 2.** The results of our FRB gravitational lensing forecasts for four surveys, assuming five years of operation with  $\sim 80\%$  duty-cycle.

<sup>†</sup> The constraints on the fraction of matter in primordial black holes without a detection of FRB microlensing.

<sup>\*</sup> We take  $\Omega_{IMBH}$  to be the constraints on the density of intermediate mass black holes in the absence of a lensing detection.  $N_{lens,IMBH}$  corresponds to the expected number of FRB lensing detections with  $\Delta t$  between 1–100 seconds assuming the rate from BATSE GRBs (Paynter et al. 2021).

<sup>\*\*</sup> The expected number of detections of FRBs lensed by massive galaxies. DSA-2000, CHORD, and CHIME/FRB cannot access time delays longer than a pointing duration/transit time, so they will not see strong lensing by foreground galaxies. The CHIME/FRB stellar lensing uncertainty is large because it is not clear what fraction of total events will have preserved voltage data and high DM.

The relationship between FRB brightness and distance is critical for predicting the redshift distribution for more sensitive surveys. Fortunately for telescopes such as DSA-2000, CHORD, and FAST, there is evidence that dimmer FRBs come from higher redshifts, meaning more sensitive surveys will probe a deeper redshift distribution. This was not guaranteed, as a sufficiently flat luminosity function would result in the brightest FRBs being farther away (Macquart & Ekers 2018). The positive correlation between fluence and DM was demonstrated by Shannon et al. (2018) when comparing the Parkes  $DM_{ex}$  distribution with that of ASKAP in Fly’s eye mode. The relationship has also been borne out by the large DMs of FAST-discovered FRBs, which can detect pulses down to tens of milliJanskys (Niu et al. 2021). The exact mapping between observed fluence and redshift will depend on the FRB luminosity function, the *true* source distribution in  $z$ , and selection effects (Connor 2019), but for our purpose this simple model is adequate. We take the DM and redshift distribution of the hypothetical CASM survey to be the same as CHIME/FRB, since it will have similar parameters to CHIME but with 25 times more FoV.

In a Euclidean volume, the mean FRB distance in a given survey scales as the square-root of a survey’s sensitivity (Li et al. 2019), so cutting in half a telescope’s SEFD will lead to it detecting FRBs that are, one average,  $\sim 40\%$  farther away. For a cosmological population, the relationship is slightly weaker. We simulate  $n(z)$  for DSA-2000 and CHORD based on the modeled redshift distribution of CHIME/FRB. We assume FRBs have a constant comoving volume density and a single cumulative power-law luminosity function that has  $\gamma = 1$ .

## 4. RESULTS

### 4.1. Strong lensing by stars

Considerable attention has been paid to short-duration FRB gravitational lensing by MACHOs and PBHs (Muñoz et al. 2016; Zhou et al. 2022; Kader et al. 2022; Leung et al. 2022). To our knowledge, nobody has considered strong lensing of FRBs by stars in the cosmological context. Stars at  $z_l = 0.5$  will have an Einstein radius of  $\theta_E \approx 1.6'' \times \left(\frac{M}{M_{\odot}}\right)^{1/2}$  for a source at  $z_s = 1$ . This corresponds to a physical impact parameter of roughly  $10^{16}$  cm, much larger than stellar radii. The geometry gives a fiducial lensing timescale of 20 microseconds per solar mass, which is already within the region of lags that CHIME/FRB is capable of searching (Kader et al. 2022; Leung et al. 2022). If the cosmological stellar density parameter is  $\Omega_* \approx 0.0025$ , then this is equivalent to  $f_* = \frac{\Omega_*}{\Omega_c} \approx 10^{-2}$  (Fukugita & Peebles 2004; Aghanim et al. 2020). From Figure 3, we see that the optical depth for such a population of point-masses is significant, even for a relatively nearby CHIME/FRB catalog.

However, unlike PBHs and MACHOs, stars are highly concentrated near the cores of galaxies. Wyithe & Turner (2002) have shown that the strong spatial clustering of stars renders the Press-Gunn approximation inadequate for cosmological stellar microlensing. In other words, if the isolated lens assumptions is broken and  $\tau$  approaches or exceeds 1, point-mass lenses may be over-counted (Koopmans & Wambsganss 2001). An extreme example is if stellar lenses in the Universe were all aligned radially; the probability of strong microlensing would be effectively zero. Wyithe

& Turner (2002) found that roughly 1% of sources at or beyond redshift 2 will be lensed by stars. Their work, and related papers, were in the context of GRBs, where multiple copies from stellar microlensing cannot be detected unless the delay is longer than the burst width. FRBs do not have this issue. Here we consider how stars in elliptical and spiral galaxies will impact FRB gravitational lensing for realistic FRB redshifts, correcting for the spatial distribution of stellar mass in galaxies. In Section 4.2, we discuss how lensing by stars can be distinguished from other point-masses such as PBHs.

For our forecast of FRB stellar lensing, we make the conservative assumption that only stars within a relatively small threshold impact parameter of a foreground galaxy will contribute to the optical depth. The probability of stellar lensing is roughly 1 for sources that pass within  $\sim 3$  kpc of a Milky Way like galaxy. Such galaxies have a volumetric density of  $0.01 \text{ Mpc}^{-3}$ , which means the optical depth for stellar lensing would be  $\tau_* \approx 3 \times 10^{-4} \left( \frac{D_l}{1 \text{ Gpc}} \right)$  for spiral galaxies. For elliptical galaxies the impact parameter within which microlensing optical depth is  $\sim 1$ , is larger. Assuming sightlines within 6 kpc of elliptical galaxies are microlensed, we find  $\tau_* \approx 10^{-3} \left( \frac{D_l}{1 \text{ Gpc}} \right)$ . This leads to the striking fact that roughly one per thousand CHIME/FRB sources could be lensed by stars on timescales between 1–100 microseconds.

Similar to strong lensing by galaxies, the majority of stellar microlensing events will be due to elliptical galaxies. Wyithe & Turner (2002) find that for spiral galaxies, roughly 70% of high- $z$  sources microlensed by stars will also be strongly lensed by the galaxy itself. For elliptical/S0 galaxies, this number is closer to half. Therefore, detecting an FRB with microsecond lensing is a good indicator that it is also lensed on days to weeks timescales and that its host galaxy will be lensed in an optical image. If the FRB source is a repeater, then the lensing system could be monitored in order to constrain  $H_0$  (Wucknitz et al. 2021).

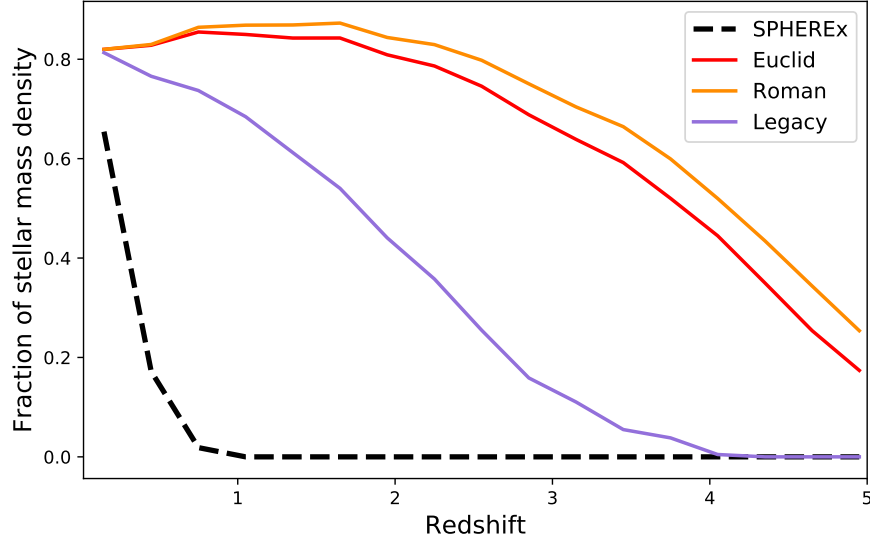
Current and future wide-area optical/IR surveys will prove excellent resources for identifying the host galaxies of stellar microlenses. The extant Legacy Survey delivers images over  $14,000 \text{ deg}^2$  with a  $1.2''$  point-spread function (PSF) FWHM in the  $g$ ,  $r$ , and  $z$  bands, detecting objects to  $g = 24.0$  and  $r = 23.4$  (Dey et al. 2019). Space-based imaging surveys with *Euclid* (Scaramella et al. 2021) will span  $15,000 \text{ deg}^2$  across several visible and near-IR bands, with detection limits of 26.2 mag in the visible and 24.5 in the near-IR, and a PSF FWHM of  $0.225''$  in the visible and  $0.3''$  pixels in the near-IR that undersample the PSF. The Nancy Grace Roman Space Telescope (Roman; Doré et al. 2018) will cover only  $2,000 \text{ deg}^2$  in the near-IR with a  $0.28''$  PSF FWHM, but will detect objects to 26.6 mag. Finally, the SPHEREx mission will deliver accurate redshifts of a few  $\times 10^8$  galaxies over the whole sky, with a detection limit of 18.4 mag in the near-IR in each spectral channel.

Figure 6 shows the fraction of the stellar mass density of the Universe recovered within each survey footprint, as a function of redshift. We used the survey detection thresholds to identify detectable galaxies at each redshift in the output catalog of a recent semi-analytic galaxy formation model based on the Millennium simulation rescaled to the latest Planck cosmology (Henriques et al. 2020). We used predicted galaxy magnitudes that included the simulated effects of internal dust extinction, and required detection in at least one band for each survey (at least one spectral channel for SPHEREx). These results suggest that a significant fraction of the host galaxies of stellar microlenses will be identified within the *Euclid* and Roman survey areas, potentially enabling modeling of the galaxy-scale lens mass distribution using the lensed FRB host galaxy, as well as studies of the distant FRB host galaxy itself. The former can be used to predict the potential observation of future images of the FRB lensed on the scale of the galaxy (e.g., Rodney et al. 2021).

Astronomers must note the risk of mis-identifying a lens galaxy as the FRB host. Lensing searches should be done on microsecond timescales to differentiate the host from the lens, especially if the extragalactic DM is larger than expected. This will affect roughly  $10^{-3}$  sight lines for typical FRB distances. Since most lenses will be elliptical galaxies but most FRB hosts appear to be star-forming, a tight association with an elliptical galaxy may suggest lensing. Such localization precision can currently be achieved for CHIME/FRB VLBI, DSA-110, ASKAP, and Meerkat (Rajwade et al. 2022). Another practical issue is that scattering in the lens galaxy may diminish the signal’s significance, particularly in the case of spiral galaxies, but less so with ellipticals.

#### 4.2. Primordial black holes

Primordial black holes (PBHs) are a theoretical class of black holes that form in the early Universe. They may form via direct collapse from primordial fluctuations, or through other mechanisms (Carr & Kühnel 2020). Unlike black holes that are formed after stellar collapse above the Tolman–Oppenheimer–Volkoff limit of  $\sim 3 M_\odot$ , PBHs can be produced with a wide range of masses. Constraining this mass spectrum is an active area of research and uses a variety of inputs,



**Figure 6.** The fraction of the cosmic stellar mass density recovered within the cones of the Legacy Survey (solid purple), the *Euclid* (solid orange) and Roman (solid red) wide-area surveys, and SPHEREx (dashed black). For SPHEREx we assume that objects must be detected in at least one spectral channel, and for the remainder of the surveys we assume that objects must be detected in at least one imaging band. See text for further details on the surveys, and the simulated galaxy catalog used to derive the results.

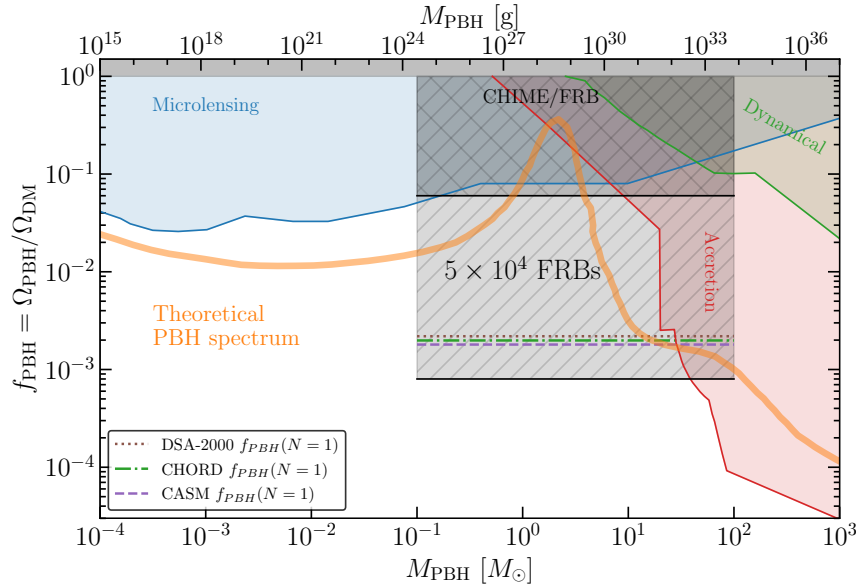


**Figure 7.** The current constraints on the mass of primordial black holes along with future constraints from FRBs. If no FRB is lensed on timescales  $1 \mu\text{s}$  to  $10 \text{ms}$ ,  $5 \times 10^4$  sources could constrain  $f_{\text{PBH}}$  to less than  $8 \times 10^{-4}$  between  $0.1$ – $100 M_{\odot}$ . If CHIME/FRB can coherently search for lensing in  $\sim 500$  unscattered FRBs, a non-detection will rule out the region  $f_{\text{PBH}}/M_{\text{PBH}}$  space that is grey and double hatched. The three horizontal lines correspond to the value of  $f_{\text{PBH}}$  that would produce on average 1 microlensing event per year from PBHs for three upcoming FRB surveys. We created this figure by modifying existing plotting code <https://github.com/bradkav/PBHbounds>.

including evaporation timescale, small-scale CMB fluctuations, and  $\text{Ly}\alpha$  forest (Carr & Kühnel 2020). For simplicity, we consider here only a monochromatic mass distribution (MMD) such that all PBHs have the same mass,  $M_{\text{PBH}}$ .

We take  $f_{\text{PBH}} \equiv \frac{\Omega_{\text{PBH}}}{\Omega_c}$  to be the fraction of cold dark matter that resides in primordial black holes, and estimate the region of  $f_{\text{PBH}}/M_{\text{PBH}}$  parameter space that current and upcoming FRB surveys will be able to search. In Figure 7

we show constraints on the abundance of primordial black holes assuming each survey will be able to detect lensing events with delays from microseconds to milliseconds ( $M_L \sim 0.1 - 100 M_\odot$ ).

We find that a non-detection from 5 years on sky with DSA-2000, CHORD, and CASM produce a similar upper-limit of  $f_{\text{PBH}} \lesssim 10^{-3}$ . While the CASM considered here would find many more FRBs, the deeper redshift distribution of DSA-2000 and CHORD result in a similar mean lensing optical depth. We plot the value of  $f_{\text{PBH}}$  that would produce an average of 1 lensed FRB per year for DSA-2000 (brown, dotted), CHORD (green, dot-dashed), and CASM (purple, dashed).

In Zhou et al. (2022), the authors calculate the  $f_{\text{PBH}}$  constraints for the non-detection of gravitational lensing in 593 CHIME/FRBs. However, their limits are weakened by the (then valid) assumption of incoherent lensing searches, where the minimum lensing delay is set by the CHIME FRB pulse width. They could not constrain PBH masses that are less than roughly  $10 M_\odot$ . The CHIME/FRB collaboration has now produced the first observational constraints from *coherent* gravitational lensing (Kader et al. 2022; Leung et al. 2022). They have used the voltage data for 172 bursts from 114 independent sightlines to constrain the fraction of dark matter in PBHs with masses between  $10^{-4}$  and  $10^4 M_\odot$ . They consider the impacts of scattering from plasma local to the source and conservatively assume that high DM events have significant dispersion in the host galaxy, putting  $\text{DM} > 500 \text{ pc cm}^{-3}$  at smaller  $z_s$ . Due to memory constraints in their data buffer, voltage data for sources with  $\text{DM} > 1000 \text{ pc cm}^{-3}$  are not included in the sample (Leung et al. 2022). The authors place an upper limit of 0.8 on  $f_{\text{PBH}}$  for  $M_{\text{PBH}} \sim 10^{-3} M_\odot$ .

CHIME/FRB has now detected over 3000 FRBs, so just  $\sim 3\%$  have gone into constraining  $f_{\text{PBH}}$  (Leung et al. 2022). If CHIME/FRB can search coherently for lensing events using the preserved voltage data of  $\sim 500$  FRBs, the PBH constraints will be given by the double-hatched grey region shown in Figure 7. We have assumed that FRBs with  $\text{DM} > 1000 \text{ pc cm}^{-3}$  or  $z_s \gtrsim 0.8$  do not contribute to the optical depth, because CHIME/FRB cannot store their voltages. For 50,000 FRBs with the same redshift distribution as CHIME/FRB, the grey singly-hatched block shows the region of  $f_{\text{PBH}}/M_{\text{PBH}}$  parameter space that will have been ruled out (i.e. several years of observing with CASM). Note our upper-limits are less conservative than those of the CHIME/FRB collaboration because we have not included instrumental and propagation effects (Kader et al. 2022; Leung et al. 2022).

There is a further practical problem associated with searching for point-mass lensing events. Lensing by stars will likely dominate in the microseconds lag range, as explained in the previous section. Therefore, with only a time-delay measurement, it will be difficult to know if a PBH has been detected rather than a stellar lensing event in an intervening galaxy. This degeneracy can be mollified—if not fully eliminated—by noting that PBHs ought to be less concentrated than stellar mass, and they will be more uniformly distributed in the cold dark matter halos of galaxies. Thus, a strong microlensing event that occurs within  $\sim 10 \text{ kpc}$  of the host galaxy center will likely be due to a star. Constraints on  $f_{\text{PBH}}$  could be limited to sources with larger impact parameters. Using the spatial offset information requires that the telescope has  $5''$  localization precision or better. At present, CHIME/FRB cannot achieve such localizations, so if there were a positive detection between  $1-100 \mu\text{s}$ , they could not attribute it to a PBH rather than a star.

#### 4.3. Intermediate mass black holes

IMBHs are black holes whose mass lies between stellar mass black holes and the supermassive black holes that reside at the centers of galaxies (Greene et al. 2020). They are often defined to have masses between  $100 M_\odot$  and  $10^5 M_\odot$ . There is currently no concrete observational evidence for their existence, though there are a number of candidates in that range (e.g. ultra-luminous X-ray sources (Kaaret et al. 2017)). Theoretically, IMBHs ought to exist in relatively high abundance, as there must be an evolutionary bridge between stellar and supermassive black holes. Directly observing IMBHs and constraining their number density is major outstanding problem in astronomy.

Lensed FRBs will probe the volumetric density of IMBHs. For a lens at redshift 0.5, the lensing time delay is between 3 ms and a few seconds for lens masses of  $10^2-10^5 M_\odot$ . We parameterize the cosmological density of IMBHs in the standard way as,

$$\Omega_{\text{IMBH}} = \frac{\rho_{\text{IMBH}}}{\rho_c}, \quad (28)$$

where  $\rho_{\text{IMBH}}$  is the mean density of IMBHs and  $\rho_c$  the critical density of the Universe,

$$\rho_c = \frac{3H_0^2}{8\pi G}. \quad (29)$$

To forecast “millilensing” events on upcoming surveys, we consider two scenarios. First, we apply a similar treatment of PBHs, where we ask how well  $\Omega_{IMBH}$  can be constrained if no FRBs are lensed on timescales of 3 ms to a few seconds. Our second approach is to assume previous candidates in the relevant mass range (Paynter et al. 2021; Vedantham et al. 2017) were true gravitational lensing events and then extrapolate from their inferred optical depths.

If no millilensing event is found, we can constrain the cosmic density of IMBHs at 90% confidence to,

$$\tau \lesssim 2.3 B^{-1} N_{FRB}^{-1}. \quad (30)$$

The factor of 2.3 is from the 90% Poissonian confidence limits, having seen zero events.  $B$  is magnification bias. We can then use the Press-Gunn relation to get,

$$\Omega_{IMBH} \lesssim 2.3 B^{-1} N_{FRB}^{-1} \left( \frac{\langle z \rangle}{2} \right)^2 \quad (31)$$

We use the modeled redshift distribution means of DSA-2000, CHORD, CASM, and CHIME/FRB to compute these upper limits. They are displayed in Table 4.

Next, we will assume that gravitationally lensed fast transients have already been observed and extrapolate rates directly from them. Paynter et al. (2021) found evidence that GRB 950830 was lensed by a  $\sim 5 \times 10^4 M_\odot$  black hole at  $z \approx 1$ . They also use the approximation (Press & Gunn 1973) that  $\Omega_{IMBH} \sim \tau(\langle z_s \rangle = 2)$  and calculate optical depth from one lensed event in  $\sim 2700$  BATSE GRBs. For a mean source redshift of  $\sim 2$  they claim,

$$\Omega_{IMBH}(M \sim 10^{4-5} M_\odot) \approx 4.6_{-3.3}^{+9.8} \times 10^{-4}. \quad (32)$$

A related result comes from “Symmetric Achromatic Variability” seen in active galaxies. Vedantham et al. (2017) proposed that the achromatic temporal variation observed in BL Lac object J1415+1320 was a millilensing event, plausibly caused by a dark matter subhalo or black hole located within an intervening galaxy. The relatively large density of IMBHs implied by GRB 950830 and J1415+1320 would be promising for upcoming FRB surveys, which will be sensitive to a wider range of lens masses and will have a larger collection of transients than BATSE. FRB lensing will be less ambiguous than GRB events, because of the coherent temporal methods described in Section 2.3. Again, we use the modeled mean redshifts of four surveys in Table 1 and the  $\tau(z_s)$  relation to estimate the optical depth from IMBHs for FRBs, scaling from the mean redshift of GRBs. We find the DSA-2000, CHORD, CASM, and CHIME/FRB will have effective optical depths that are 2.8, 4, 16, and 16 times lower than BATSE GRBs, respectively. This is because FRBs in those surveys will be more nearby than typical GRBs. We find that, contingent on GRB 950830 having been lensed, DSA-2000 will find 0.1–7.3 FRBs lensed by IMBHs after five years of observing at 80% efficiency. Similarly, CHORD will find 0.1–7.0 events, assuming the BATSE GRB was lensed and the sample’s mean redshift was roughly 2. CASM would detect 0.3–7.2 and CHIME/FRB could expect 0.01–0.29 IMBH-lensed bursts.

#### 4.4. Massive galaxy lenses

FRBs lensed by massive galaxies will experience time-delays from days to months. The FRB’s host galaxy should also be gravitationally lensed and will allow for modeling of the lensing galaxy’s mass profile. Unlike time-variable non-transient sources like quasars, the FRB is only “on” for a millisecond and will not obscure the lensed host galaxy. Furthermore, FRBs lead to time-delay uncertainties that are more than ten orders of magnitude smaller than previous applications of time-delay cosmography. For these reasons, FRB lensing by massive galaxies has been suggested as a new tool for measuring the Hubble parameter (Li et al. 2018). Wucknitz et al. (2021) even proposed using gravitational lenses as a galaxy-scale interferometer to resolve structure and motion in the FRB itself. Most of these methods require repeating FRBs to break the mass-sheet degeneracy (Falco et al. 1985). Interferometric localization will alleviate the need for temporal coherence, as the lensed FRB images could be spatially resolved for typical image separations.

The probability of detecting a lensed event whose delay is longer than a survey pointing time or a transit time ( $\sim 10^3$  s for DSA-2000, CHORD, and CHIME/FRB), is very low. If a telescope is always pointing at the same patch of sky, either because it is ultra-widefield (a CASM such as BURSTT) or through special survey strategy, it can in principle detect lensing delays up to the survey duration ( $\sim$  years). For this reason, we consider only CASM when forecasting detection rates of FRB lensing by massive galaxies.

We use the lensing rate formalism presented in Equation 5 to estimate the number of FRBs lensed by massive galaxies. We take the magnification bias for an SIS dark matter halo and source power-law luminosity function with

cumulative index  $\gamma = 1$ . We find that after five years of observing, our putative CASM would detect 5–40 FRBs lensed by massive galaxies. The lower limit comes from assuming no magnification bias and 12,500 CASM FRB detections per year. The upper bound assumes  $\gamma = 1.0$  and  $B = 4$  with 25,000 FRBs per year

#### 4.5. Probing the circumgalactic medium

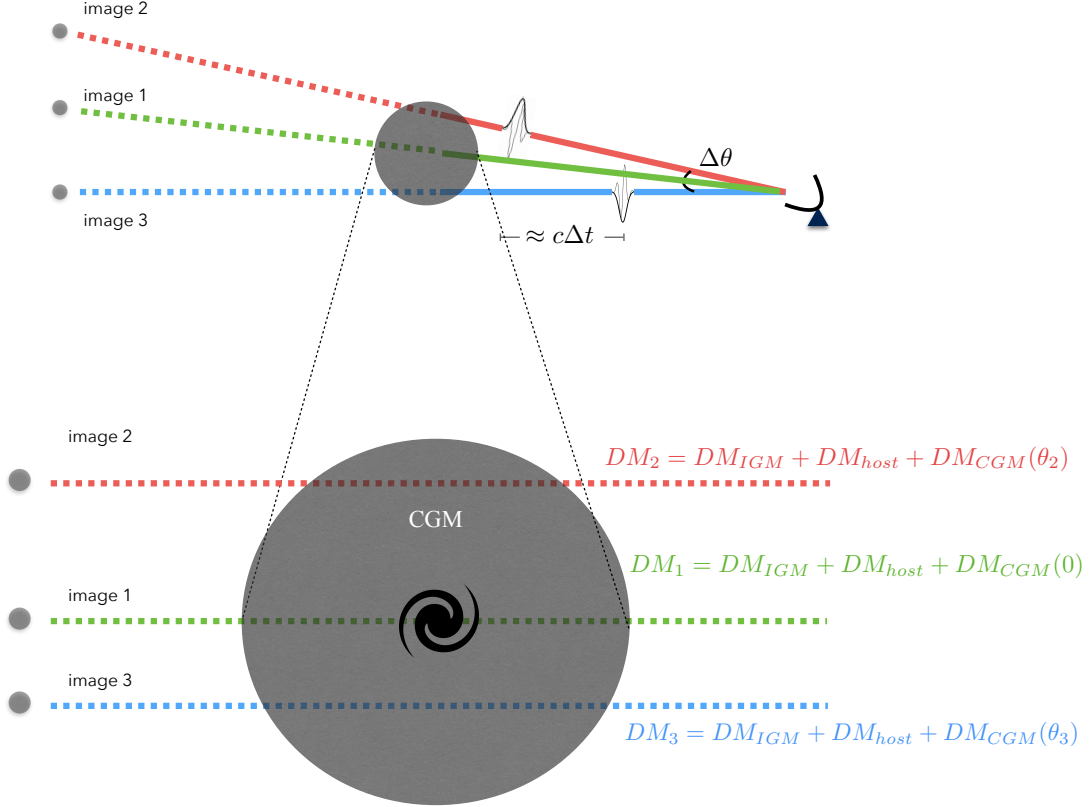


**Figure 8.** A schematic diagram of using gravitationally lensed FRBs as probes of the circumgalactic medium of lensing galaxies. Each image will have the same host DM, IGM DM, and contribution from the Milky Way, so the only difference in observed DM between multiple copies will be attributable to the lensing galaxy’s CGM.

Most proposed methods studying the circumgalactic medium (CGM) using FRBs have relied on the ensemble statistics of large numbers of sources, using DM and its line-of-sight statistics to study the distribution halo gas (McQuinn 2014; Connor & Ravi 2021). Another approach is to model the contribution to DM from the host galaxy, the intergalactic medium (IGM), and the Milky Way to infer the component imparted by the halos of intervening galaxies (Prochaska et al. 2019; Ravi 2019). Both approaches are limited by modelling uncertainties. But an FRB lensed by a massive intervening galaxy will probe that galaxy’s halo gas along multiple sight-lines. This would be a clean measure of that galaxy’s CGM, as the only difference in propagation for the multiple paths will arise due to the galaxy lens. The method would constrain both the radial profile of halo gas density, as well as the CGM’s inhomogeneity. A diagram of this idea is shown in Figure 8.

A similar technique has been used for many years in quasar absorption studies, where multiply-imaged quasars have been used to measure the structure and differential composition of the CGM of intervening lensing galaxies (Rauch 2002), even on spatial scales as small as 400 pc (Rudie et al. 2019). However, such studies measure metal-bearing gas and cannot easily constrain the total baryonic matter in the halo, due to large uncertainties when extrapolating from the relatively rare metals to total gas content.

With strong lensing of an FRB detected with very long baseline interferometry (VLBI), the halo of the galaxy lens could be studied directly by comparing the DM, RM, and scattering properties of the multiple copies. Even if the lensing galaxy is a massive elliptical, Zahedy et al. (2019) has shown that such quiescent halos still have a rich

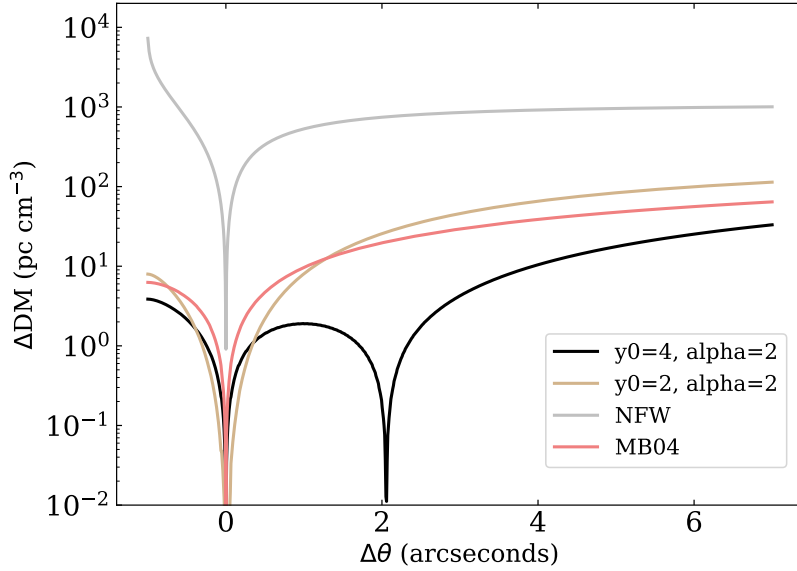


**Figure 9.** The observed difference in DM between two copies of an FRB lensed by a  $10^{12} M_{\odot}$  galaxy.  $\Delta\text{DM}$  is plotted as a function of image separation,  $\Delta\theta$ , assuming the first image is at  $\theta_1 = 1''$ . We have used four simple, spherically symmetric models for the free electron distribution in the lensing galaxy CGM. The  $y_0 = 4$  curve has two zero points because its DM curve is non-monotonic.

CGM. We assume that the angular positions of the lensed copies can be measured to  $\lesssim 0.25$  arcseconds with VLBI outriggers. From this, one would have both the angular separation of the lenses images and the lensing time-delay. VLBI localization would give the angular impact parameter,  $\theta$ , allowing one to determine where in the intervening galaxy's halo the FRB passed through. The DM from an intervening halo will be given by the following integral,

$$\text{DM}_{CGM} = 2 \int_0^{\sqrt{r_{max}^2 - b^2}} \frac{n_e(r)}{1 + z_l} dr, \quad (33)$$

where  $r_{max}$  is a halo cutoff radius, which we will take to be the virial radius,  $r_{200}$ , and,

$$b \approx \theta D_l. \quad (34)$$

The observed quantity is the difference in DM between the two images. This is given by the difference in sightlines from the lensing galaxy's CGM,  $\Delta\text{DM} = \text{DM}_{CGM}(\theta_1) - \text{DM}_{CGM}(\theta_2)$  given by,

$$\Delta\text{DM} = \frac{2}{1 + z_l} \int_{r_2}^{r_1} n_e(r) dr. \quad (35)$$

Here we have written  $\Delta\text{DM}$  as a single definite integral with  $r_1 = \sqrt{r_{max}^2 - \theta_1^2 D_l^2}$  and  $r_2 = \sqrt{r_{max}^2 - \theta_2^2 D_l^2}$ . At present, we do not know  $n_e(r)$ . But we will have measured  $\Delta\text{DM}$ , the lens redshift,  $z_l$ , and  $\theta_1$  and  $\theta_2$ . In Figure 9 we plot  $\Delta\text{DM}$  for a range of  $\Delta\theta$ , holding  $\theta_1$  fixed at  $1''$ . We use four models from Prochaska & Zheng (2019), but this a non-exhaustive list. The first is a classic Navarro-Frenk-White (NFW) profile (Navarro et al. 1997), which can be generalized to an modified NFW (mNFW) profile as,

$$\rho(r) = \frac{\rho_b}{y^{1-\alpha} (y_0 + y)^{2+\alpha}}, \quad (36)$$

with  $y \equiv c \frac{r}{r_{200}}$  where  $r$  is radius,  $r_{200}$  is the virial radius, and  $c$  is a concentration parameter. For the standard NFW,  $\alpha = 0$  and  $y_0 = 1$ . We also consider two mNFWs with  $(y_0 = 2, \alpha = 2)$  and  $(y_0 = 4, \alpha = 2)$ . The final model, MB04, comes from [Maller & Bullock \(2004\)](#). The DMs and halo models were calculated with publicly available code<sup>3</sup>.

The NFW profile is unrealistically steep at small radii, leading to large DM differences even for small angular separations (see Figure 9). The other three models are distinguishable for  $\Delta\theta \geq 0.5''$ , since observed FRB DM uncertainties with voltage data are often less than  $0.5 \text{ pc cm}^{-3}$ . Combining  $\Delta\text{DM}$  with the difference in rotation measure,  $\Delta\text{RM}$ , will give a clean measure of the CGM line-of-sight magnetic field difference between the two impact parameters. This measurement will be valuable because the magnetic field in galaxy halos remains largely unconstrained observationally ([van de Voort et al. 2021](#)).

## 5. CONCLUSIONS

Fast radio bursts offer a unique probe of the Universe’s dark matter via gravitational lensing, thanks to their abundance, short duration, and the coherent nature of their detection. In principle, FRBs can give us access to  $\sim$  fifteen orders of magnitude in lens mass, corresponding to lensing time delays of microseconds to years. This is made possible by saving phase-preserving voltage data (the electric field waveform of the radio pulse itself). We have provided an overview of FRB gravitational lensing spanning a wide range of time-delays and lens masses. We have forecasted detection rates for upcoming and current surveys. These include DSA-2000, CHORD, a coherent all-sky monitor (CASM) such as BURSTT, as well as CHIME/FRB, which is currently finding large numbers of FRBs and searching for lensing events. The FRB redshift distribution is critical to any lensing optical depth calculation because lensing probability is a strong function of source distance. This creates a trade-off between deep, sensitive telescopes such as DSA-2000 and CHORD, and ultra-widefield but less sensitive CASM surveys.

On 1–100 microseconds timescales, FRBs will be lensed by stars in foreground galaxies at a significant rate and could plausibly be detected by CHIME/FRB. If lensing by stars can be distinguished from compact dark objects, FRB surveys will limit the abundance of primordial black holes in the mass range  $0.1\text{--}100 M_{\odot}$ . This mass range is under-explored and is favoured by some theorists to be the most relevant mass scale for PBHs ([Carr & Kühnel 2020](#)). All surveys we have considered will also constrain the cosmological density of intermediate mass black holes,  $\Omega_{IMBH}$ . If recent claims of GRB millilensing by IMBHs ([Paynter et al. 2021](#)) are correct, DSA-2000, CHORD, and the putative CASM survey could all detect a few lensed FRBs on timescales of 0.01–10 s over the course of their surveys. On longer delay timescales (days to years), FRBs will be lensed by massive galaxies. Several cosmological applications have been proposed for these systems ([Li et al. 2018](#); [Wucknitz et al. 2021](#)). Detecting strong lensing by galaxies is difficult because it is not known when the lensed copy will arrive, so the radio telescope must be pointing at the same location most of the time. Of the telescopes and survey strategies considered here, only a CASM-like survey (e.g. a BURSTT-like telescope but with a CHIME/FRB SEFD) could plausibly find FRB lensing by massive galaxies, with 5–40 such events after five years of observing.

Finally, we have proposed a new method for studying the circumgalactic medium of lensing galaxies. Multiply imaged FRBs will traverse the lensing halos’ CGM at different impact parameters and will be differentially dispersed, Faraday rotated, or even scattered. Unlike with previous methods, this provides a clean model-independent measure of the total baryonic material in dark matter halos as a function of radius. Our method requires sub-arcsecond localization of each lensed copy of the FRB, which will only be possible for CASM-like surveys that have VLBI outriggers.

**Data availability statement** This work was based on publicly available data and can be reproduced with the Jupyter notebook found in <https://github.com/liamconnor/frb-grav-lensing>.

<sup>1</sup> We thank Sterl Phinney and Minghao Yue for valuable insights on strong lensing. We also thank Matt Dobbs, Keith Vanderlinde, Zarif Kader, and Ue-Li Pen for helpful discussions on coherent gravitational lensing.

<sup>3</sup> <https://github.com/FRBs/FRB>

## REFERENCES

- Aghanim, N., Akrami, Y., Ashdown, M., et al. 2020, *Astronomy & Astrophysics*, 641, A6
- Bannister, K. W., Deller, A. T., Phillips, C., et al. 2019, *Science*, 365, 565, doi: [10.1126/science.aaw5903](https://doi.org/10.1126/science.aaw5903)
- Carr, B., & Kühnel, F. 2020, *Annual Review of Nuclear and Particle Science*, 70, 355, doi: [10.1146/annurev-nucl-050520-125911](https://doi.org/10.1146/annurev-nucl-050520-125911)
- Chen, X., Shu, Y., Li, G., & Zheng, W. 2021a, *ApJ*, 923, 117, doi: [10.3847/1538-4357/ac2c76](https://doi.org/10.3847/1538-4357/ac2c76)
- Chen, X., Shu, Y., Zheng, W., & Li, G. 2021b, *ApJ*, 912, 134, doi: [10.3847/1538-4357/abf119](https://doi.org/10.3847/1538-4357/abf119)
- CHIME/FRB Collaboration, Amiri, M., Bandura, K., et al. 2018, *ApJ*, 863, 48, doi: [10.3847/1538-4357/aad188](https://doi.org/10.3847/1538-4357/aad188)
- CHIME/FRB Collaboration, Amiri, M., Andersen, B. C., et al. 2021, *ApJS*, 257, 59, doi: [10.3847/1538-4365/ac33ab](https://doi.org/10.3847/1538-4365/ac33ab)
- Connor, L. 2019, *MNRAS*, 487, 5753, doi: [10.1093/mnras/stz1666](https://doi.org/10.1093/mnras/stz1666)
- Connor, L., & Ravi, V. 2021, arXiv e-prints, arXiv:2107.13692. <https://arxiv.org/abs/2107.13692>
- Cordes, J. M., & Chatterjee, S. 2019, *ARA&A*, 57, 417, doi: [10.1146/annurev-astro-091918-104501](https://doi.org/10.1146/annurev-astro-091918-104501)
- Dey, A., Schlegel, D. J., Lang, D., et al. 2019, *AJ*, 157, 168, doi: [10.3847/1538-3881/ab089d](https://doi.org/10.3847/1538-3881/ab089d)
- Doré, O., Hirata, C., Wang, Y., et al. 2018, arXiv e-prints, arXiv:1804.03628. <https://arxiv.org/abs/1804.03628>
- Eichler, D. 2017, *ApJ*, 850, 159, doi: [10.3847/1538-4357/aa8b70](https://doi.org/10.3847/1538-4357/aa8b70)
- Falco, E. E., Gorenstein, M. V., & Shapiro, I. I. 1985, *ApJL*, 289, L1, doi: [10.1086/184422](https://doi.org/10.1086/184422)
- Fukugita, M., & Peebles, P. J. E. 2004, *ApJ*, 616, 643, doi: [10.1086/425155](https://doi.org/10.1086/425155)
- Greene, J. E., Strader, J., & Ho, L. C. 2020, *ARA&A*, 58, 257, doi: [10.1146/annurev-astro-032620-021835](https://doi.org/10.1146/annurev-astro-032620-021835)
- Hallinan, G., Ravi, V., Weinreb, S., et al. 2019, in *Bulletin of the American Astronomical Society*, Vol. 51, 255. <https://arxiv.org/abs/1907.07648>
- Hashimoto, T., Goto, T., On, A. Y. L., et al. 2020, *MNRAS*, 497, 4107, doi: [10.1093/mnras/staa2238](https://doi.org/10.1093/mnras/staa2238)
- Henriques, B. M. B., Yates, R. M., Fu, J., et al. 2020, *MNRAS*, 491, 5795, doi: [10.1093/mnras/stz3233](https://doi.org/10.1093/mnras/stz3233)
- James, C. W., Prochaska, J. X., Macquart, J. P., et al. 2022, *MNRAS*, 509, 4775, doi: [10.1093/mnras/stab3051](https://doi.org/10.1093/mnras/stab3051)
- James, C. W., Bannister, K. W., Macquart, J. P., et al. 2019, *PASA*, 36, e009, doi: [10.1017/pasa.2019.1](https://doi.org/10.1017/pasa.2019.1)
- Jow, D. L., Foreman, S., Pen, U.-L., & Zhu, W. 2020, *MNRAS*, 497, 4956, doi: [10.1093/mnras/staa2230](https://doi.org/10.1093/mnras/staa2230)
- Kaaret, P., Feng, H., & Roberts, T. P. 2017, *ARA&A*, 55, 303, doi: [10.1146/annurev-astro-091916-055259](https://doi.org/10.1146/annurev-astro-091916-055259)
- Kader, Z., Leung, C., Dobbs, M., et al. 2022, arXiv e-prints, arXiv:2204.06014. <https://arxiv.org/abs/2204.06014>
- Kant, G. W., van der Wal, E., Ruiter, M., & Benthem, P. 2009, in *Wide Field Astronomy & Technology for the Square Kilometre Array*, 37
- Kelly, P. L., Rodney, S. A., Treu, T., et al. 2015, *Science*, 347, 1123, doi: [10.1126/science.aaa3350](https://doi.org/10.1126/science.aaa3350)
- Koopmans, L. V. E., & Wambsganss, J. 2001, *MNRAS*, 325, 1317, doi: [10.1046/j.1365-8711.2001.04279.x](https://doi.org/10.1046/j.1365-8711.2001.04279.x)
- Leung, C., Kader, Z., Masui, K. W., et al. 2022, arXiv e-prints, arXiv:2204.06001. <https://arxiv.org/abs/2204.06001>
- Li, D., Yalinewich, A., & Breyse, P. C. 2019, arXiv e-prints, arXiv:1902.10120. <https://arxiv.org/abs/1902.10120>
- Li, Z.-X., Gao, H., Ding, X.-H., Wang, G.-J., & Zhang, B. 2018, *Nature Communications*, 9, 3833, doi: [10.1038/s41467-018-06303-0](https://doi.org/10.1038/s41467-018-06303-0)
- Lin, H.-H., Lin, K.-y., Li, C.-T., et al. 2022, arXiv e-prints, arXiv:2206.08983. <https://arxiv.org/abs/2206.08983>
- Macquart, J. P., & Ekers, R. 2018, *MNRAS*, 480, 4211, doi: [10.1093/mnras/sty2083](https://doi.org/10.1093/mnras/sty2083)
- Macquart, J. P., Prochaska, J. X., McQuinn, M., et al. 2020, *Nature*, 581, 391, doi: [10.1038/s41586-020-2300-2](https://doi.org/10.1038/s41586-020-2300-2)
- Main, R., van Kerkwijk, M., Pen, U.-L., Mahajan, N., & Vanderlinde, K. 2017, *ApJL*, 840, L15, doi: [10.3847/2041-8213/aa6f03](https://doi.org/10.3847/2041-8213/aa6f03)
- Maller, A. H., & Bullock, J. S. 2004, *MNRAS*, 355, 694, doi: [10.1111/j.1365-2966.2004.08349.x](https://doi.org/10.1111/j.1365-2966.2004.08349.x)
- McQuinn, M. 2014, *ApJL*, 780, L33, doi: [10.1088/2041-8205/780/2/L33](https://doi.org/10.1088/2041-8205/780/2/L33)
- Michilli, D., Masui, K. W., Mckinven, R., et al. 2021, *ApJ*, 910, 147, doi: [10.3847/1538-4357/abe626](https://doi.org/10.3847/1538-4357/abe626)
- Muñoz, J. B., Kovetz, E. D., Dai, L., & Kamionkowski, M. 2016, *PhRvL*, 117, 091301, doi: [10.1103/PhysRevLett.117.091301](https://doi.org/10.1103/PhysRevLett.117.091301)
- Narayan, R., & Bartelmann, M. 1996, arXiv e-prints, astro. <https://arxiv.org/abs/astro-ph/9606001>
- Navarro, J. F., Frenk, C. S., & White, S. D. M. 1997, *ApJ*, 490, 493, doi: [10.1086/304888](https://doi.org/10.1086/304888)
- Niu, C.-H., Li, D., Luo, R., et al. 2021, *ApJL*, 909, L8, doi: [10.3847/2041-8213/abe7f0](https://doi.org/10.3847/2041-8213/abe7f0)
- Oguri, M. 2019, *Reports on Progress in Physics*, 82, 126901, doi: [10.1088/1361-6633/ab4fc5](https://doi.org/10.1088/1361-6633/ab4fc5)
- Paynter, J., Webster, R., & Thrane, E. 2021, *Nature Astronomy*, 5, 560, doi: [10.1038/s41550-021-01307-1](https://doi.org/10.1038/s41550-021-01307-1)
- Pen, U.-L. 2018, *Nature Astronomy*, 2, 842, doi: [10.1038/s41550-018-0620-z](https://doi.org/10.1038/s41550-018-0620-z)

- Peterson, J. B., Bandura, K., & Pen, U. L. 2006, arXiv e-prints, astro. <https://arxiv.org/abs/astro-ph/0606104>
- Petroff, E., Hessels, J. W. T., & Lorimer, D. R. 2019, *A&A Rv*, 27, 4, doi: [10.1007/s00159-019-0116-6](https://doi.org/10.1007/s00159-019-0116-6)
- Press, W. H., & Gunn, J. E. 1973, *ApJ*, 185, 397, doi: [10.1086/152430](https://doi.org/10.1086/152430)
- Prochaska, J. X., & Zheng, Y. 2019, *MNRAS*, 485, 648, doi: [10.1093/mnras/stz261](https://doi.org/10.1093/mnras/stz261)
- Prochaska, J. X., Macquart, J.-P., McQuinn, M., et al. 2019, *Science*, 366, 231, doi: [10.1126/science.aay0073](https://doi.org/10.1126/science.aay0073)
- Rajwade, K. M., Bezuidenhout, M. C., Caleb, M., et al. 2022, *MNRAS*, 514, 1961, doi: [10.1093/mnras/stac1450](https://doi.org/10.1093/mnras/stac1450)
- Rauch, M. 2002, in *Astronomical Society of the Pacific Conference Series*, Vol. 254, *Extragalactic Gas at Low Redshift*, ed. J. S. Mulchaey & J. T. Stocke, 140. <https://arxiv.org/abs/astro-ph/0111032>
- Ravi, V. 2019, *ApJ*, 872, 88, doi: [10.3847/1538-4357/aafb30](https://doi.org/10.3847/1538-4357/aafb30)
- Refsdal, S. 1964, *MNRAS*, 128, 307, doi: [10.1093/mnras/128.4.307](https://doi.org/10.1093/mnras/128.4.307)
- Rodney, S. A., Brammer, G. B., Pierel, J. D. R., et al. 2021, *Nature Astronomy*, 5, 1118, doi: [10.1038/s41550-021-01450-9](https://doi.org/10.1038/s41550-021-01450-9)
- Rudie, G. C., Steidel, C. C., Pettini, M., et al. 2019, *ApJ*, 885, 61, doi: [10.3847/1538-4357/ab4255](https://doi.org/10.3847/1538-4357/ab4255)
- Scaramella, R., Amiaux, J., Mellier, Y., et al. 2021, arXiv e-prints, arXiv:2108.01201. <https://arxiv.org/abs/2108.01201>
- Shannon, R. M., Macquart, J. P., Bannister, K. W., et al. 2018, *Nature*, 562, 386, doi: [10.1038/s41586-018-0588-y](https://doi.org/10.1038/s41586-018-0588-y)
- Suyu, S. H., Bonvin, V., Courbin, F., et al. 2017, *MNRAS*, 468, 2590, doi: [10.1093/mnras/stx483](https://doi.org/10.1093/mnras/stx483)
- Tegmark, M., & Zaldarriaga, M. 2009, *PhRvD*, 79, 083530, doi: [10.1103/PhysRevD.79.083530](https://doi.org/10.1103/PhysRevD.79.083530)
- Treu, T., & Marshall, P. J. 2016, *A&A Rv*, 24, 11, doi: [10.1007/s00159-016-0096-8](https://doi.org/10.1007/s00159-016-0096-8)
- Turner, E. L. 1980, *ApJL*, 242, L135, doi: [10.1086/183418](https://doi.org/10.1086/183418)
- van de Voort, F., Bieri, R., Pakmor, R., et al. 2021, *MNRAS*, 501, 4888, doi: [10.1093/mnras/staa3938](https://doi.org/10.1093/mnras/staa3938)
- van Leeuwen, J., Kooistra, E., Oostrum, L., et al. 2022, arXiv e-prints, arXiv:2205.12362. <https://arxiv.org/abs/2205.12362>
- Vanderlinde, K., Liu, A., Gaensler, B., et al. 2019, in *Canadian Long Range Plan for Astronomy and Astrophysics White Papers*, Vol. 2020, 28, doi: [10.5281/zenodo.3765414](https://doi.org/10.5281/zenodo.3765414)
- Vanderriest, C., Schneider, J., Herpe, G., et al. 1989, *A&A*, 215, 1
- Vedantham, H. K., Readhead, A. C. S., Hovatta, T., et al. 2017, *ApJ*, 845, 89, doi: [10.3847/1538-4357/aa745c](https://doi.org/10.3847/1538-4357/aa745c)
- Wucknitz, O., Spitler, L. G., & Pen, U. L. 2021, *A&A*, 645, A44, doi: [10.1051/0004-6361/202038248](https://doi.org/10.1051/0004-6361/202038248)
- Wyithe, J. S. B., & Turner, E. L. 2002, *ApJ*, 567, 18, doi: [10.1086/338426](https://doi.org/10.1086/338426)
- Yue, M., Fan, X., Yang, J., & Wang, F. 2022, *ApJ*, 925, 169, doi: [10.3847/1538-4357/ac409b](https://doi.org/10.3847/1538-4357/ac409b)
- Zahedy, F. S., Chen, H.-W., Johnson, S. D., et al. 2019, *MNRAS*, 484, 2257, doi: [10.1093/mnras/sty3482](https://doi.org/10.1093/mnras/sty3482)
- Zheng, Z., Ofek, E. O., Kulkarni, S. R., Neill, J. D., & Juric, M. 2014, *ApJ*, 797, 71, doi: [10.1088/0004-637X/797/1/71](https://doi.org/10.1088/0004-637X/797/1/71)
- Zhou, H., Li, Z., Huang, Z., Gao, H., & Huang, L. 2022, *MNRAS*, doi: [10.1093/mnras/stac139](https://doi.org/10.1093/mnras/stac139)